Structure
Article

The Structure of the Coiled-Coil Domain of Ndel1 and the Basis of Its Interaction with Lis1, the Causal Protein of Miller-Dieker Lissencephaly

Urszula Derewenda,[1,6] Cataldo Tarricone,[2,3,6] Won Chan Choi,[1] David R. Cooper,[1] Steve Lukasik,[4] Franco Perrina,[2,3,7] Ashutosh Tripathy,[5] Myung Hee Kim,[1,8] David S. Cafiso,[4] Andrea Musacchio,[2,3,*] and Zygmunt S. Derewenda[1,*]

[1]Department of Molecular Physiology and Biological Physics, University of Virginia, Charlottesville, VA 22908, USA
[2]Department of Experimental Oncology, European Institute of Oncology, Via Ripamonti 435, 20141 Milan, Italy
[3]Research Unit of the Italian Institute of Technology (IIT) Foundation at the IFOM-IEO Campus, Via Adamello 16, I-20139 Milan, Italy
[4]Department of Chemistry, University of Virginia, Charlottesville, VA 22904, USA
[5]Department of Biochemistry and Biophysics, University of North Carolina at Chapel Hill, Chapel Hill, NC 27599, USA
[6]These authors contributed equally to this work.
[7]Present address: MRC Laboratory of Molecular Biology, Hills Road, Cambridge CB2 0QH, United Kingdom.
[8]Present address: Systems Microbiology Research Center, KRIBB, Daejeon 305-806, Korea.
*Correspondence: zsd4n@virginia.edu (Z.S.D.), andrea.musacchio@ifom-ieo-campus.it (A.M.)
DOI 10.1016/j.str.2007.09.015

SUMMARY

Ndel1 and Nde1 are homologous and evolutionarily conserved proteins, with critical roles in cell division, neuronal migration, and other physiological phenomena. These functions are dependent on their interactions with the retrograde microtubule motor dynein and with its regulator Lis1—a product of the causal gene for isolated lissencephaly sequence (ILS) and Miller-Dieker lissencephaly. The molecular basis of the interactions of Ndel1 and Nde1 with Lis1 is not known. Here, we present a crystallographic study of two fragments of the coiled-coil domain of Ndel1, one of which reveals contiguous high-quality electron density for residues 10–166, the longest such structure reported by X-ray diffraction at high resolution. Together with complementary solution studies, our structures reveal how the Ndel1 coiled coil forms a stable parallel homodimer and suggest mechanisms by which the Lis1-interacting domain can be regulated to maintain a conformation in which two supercoiled α helices cooperatively bind to a Lis1 homodimer.

INTRODUCTION

Cytoplasmic dynein 1 is a ubiquitous retrograde motor that generates force toward the (−) end of microtubules and is involved in chromosome capture and segregation during mitosis, mitotic spindle control, transport of organelles, as well as nuclear and cell migration (Hook and Vallee, 2006; Marx et al., 2005; Vallee et al., 2004). Most, if not all of these functions, depend on the interaction of dynein with the 1.2 MDa complex dynactin (Schroer, 2004). Sophisticated regulation is required for proper loading of the dynein/dynactin complex on the (+) end of microtubules and for the attachment of the cargo. One of the key dynein binding partners is Lis1, a product of a causal gene for isolated lissencephaly sequence (ILS) and for the more severe Miller-Dieker lissencephaly (Coquelle et al., 2002; Reiner et al., 1993). These developmental syndromes are due to impaired mitotic progression of neuronal progenitor cells and to subsequent defective migration of surviving neurons, leading to a "smooth brain" phenotype associated with severe mental retardation and epilepsy (Dobyns et al., 1993; Dobyns and Truwit, 1995; Hatten, 2005; Jones et al., 1980; Reiner et al., 1993; Tsai et al., 2005). Lis1 interacts with dynein substoichiometrically, and the exact mechanism governing the interplay is not known (Faulkner et al., 2000; Sasaki et al., 2000; Smith et al., 2000; Tai et al., 2002). The dynein-related functions of Lis1 are in turn dependent on other proteins, such as the mammalian orthologs Ndel1 (formerly NudEL) and Nde1 (formerly NudE). Both these proteins, which share about ~50% amino acid sequence identity, bind directly to Lis1. Like Lis1, these proteins are highly conserved in evolution (Beckwith et al., 1995; Morris, 2000, 2003; Morris et al., 1995; Xiang and Fischer, 2004).

It is probable that all Lis1 bound to dynein/dynactin is associated directly with either Nde1 or Ndel1 (Li et al., 2005; Niethammer et al., 2000; Sasaki et al., 2000; Shu et al., 2004). Nde1 and Ndel1 appear to have physiologically distinct roles. Nde1 is localized to the centrosome and directs γ-tubulin localization and microtubule organization in interphase cells and is essential for centrosome duplication and mitotic spindle assembly (Feng et al., 2000; Feng and Walsh, 2004). Ndel1, on the other hand,

appears to regulate cortical neuronal positioning (Shu et al., 2004), and loss of Ndel1 results in neuronal migration defects and early embryonic lethality (Sasaki et al., 2005). Recently, both Ndel1 and Nde1 were identified at kinetochores, to which they localize due to an interaction with the kinetochore protein CENP-F (Stehman et al., 2007; Vergnolle and Taylor, 2007).

Ndel1 is a 345 residue long protein with a predicted coiled-coil domain spanning approximately the N-terminal 200 amino acids and a C-terminal fragment and is largely unstructured as can be inferred from amino acid composition and sequence, with a number of potential phosphorylation sites, some of which have been experimentally shown to serve as substrates for Cdk5, Cdc2, Cdk1, Aurora-A, and possibly other kinases (Mori et al., 2007; Niethammer et al., 2000; Toyo-Oka et al., 2005; Toyo-oka et al., 2003; Yan et al., 2003). Phosphorylation of the C-terminal domain is thought to regulate the interaction of Ndel1 with other proteins, including 14-3-3ε (Toyo-oka et al., 2003), DISC1 (Disrupted-In-Schizophrenia-1) (Brandon et al., 2004; Morris et al., 2003a), and katanin p60 (Toyo-Oka et al., 2005). Neither the structural bases of these interactions nor the mechanisms by which they modulate Lis1/dynein/dynactin pathways are known.

Ndel1 was shown to be dimeric in solution and in this state, associates with Lis1 to form a heterotetramer $Lis1_2/Ndel1_2$ (Tarricone et al., 2004). The structural basis of this interaction is not known, although it has been established that it is mediated by the coiled-coil domain of Ndel1 and not by the unstructured C-terminal fragment.

In this paper, we report two independently determined crystal structures of the Ndel1 coiled coil, i.e., that of a fragment containing residues 58–169 ($Ndel1^{58–169}$) and one encompassing the entire predicted coiled coil domain ($Ndel1^{8–192}$). We show that Ndel1 forms a double-stranded, parallel coiled coil. Using site-directed spin labeling and binding assays, we show that the coiled coil binds the dimeric full-length Lis1 via epitopes in the C-terminal portions of both α helices. The structure and dynamics of the coiled-coil domain suggest possible regulatory mechanisms by which the Lis1/Ndel1 complex may be regulated in vivo by phosphorylation and/or accessory proteins.

RESULTS AND DISCUSSION

Overview of the Crystal Structures

We expressed and purified several recombinant fragments of Ndel1 of which two—$Ndel1^{58–169}$ and $Ndel1^{8–192}$—gave well-diffracting crystals. Since neither contained Met residues, and heavy atom derivatives failed to yield phasing, we generated double mutants $Ndel1^{58–169(V134→M,L153→M)}$ and $Ndel1^{8–192\ (L24→M,V134→M)}$, which were used to obtain SeMet-labeled crystals. These mutants—in part based on sequence alignment with Nde1, which has methionines at positions 24 and 134—both retained the ability to bind Lis1, as assessed by pull-down assays (data not shown). The two structures were independently solved and refined at 2.1 Å and 2.3 Å resolution, respectively, with R/R_{free} values of 0.23/0.31 and 0.25/0.29 (Table 1).

Both crystal structures reveal identical homotetrameric architectures in which two monomers, A and A′, each made up of a single contiguous α-helix, dimerize in a parallel fashion via a tight coiled coil extending to Val96, and then interact with another dimer (B/B′) in a tail-to-tail fashion forming an antiparallel four-stranded bundle (Figure 1). This architecture is faithfully reproduced in the two structures despite different crystal contacts and different lengths of the constructs, suggesting that the tail-to-tail interaction of the dimer is not merely a crystallographic artifact, but that it represents one of the states of the molecule in solution.

In the $Ndel1^{8–192}$ crystal structure, the tetramer is formed by two noncrystallographic homodimers related by the crystallographic two-fold axis (Figure 1A). The two crystallographically independent monomers—A and A′—have interpretable electron density for residues 9–164 and 9–166, respectively. The entire parallel homodimer in the $Ndel1^{8–192}$ structure is ~245 Å long and only ~22 Å wide in its broadest part, making it, to the best of our knowledge, the longest coiled-coil structure ever determined at high resolution and significantly longer than the recently reported ~211 Å long midregion fragment (residues 89–208) of tropomyosin, refined at 2.3 Å resolution (Brown et al., 2005).

In the $Ndel1^{58–169}$ structure, a complete homotetramer occupies an asymmetric unit (Figure 1B). Interpretable electron density is observed for all residues with the exception of the C-terminal Arg169. Except for some differences in the compactness of the four-helix bundle, as described below, this structure is virtually identical to the respective fragment of the longer $Ndel1^{8–192}$ structure.

The hallmark of a coiled coil is a repeat of seven amino acids—a heptad—typically denoted as ***abcdefg***, with ***a*** and ***d*** residues of hydrophobic nature, often leucines, interlocking with the neighboring α-helix in a knobs-into-holes fashion (Crick, 1953; Lupas, 1996; Lupas and Gruber, 2005). Although the motif can often be inferred from sequence alone, full characterization of the coiled-coil stereochemistry and correct assignment of the ***a–d*** residues typically require the knowledge of the three-dimensional structure. This is particularly important for fragments that contain three or four residue insertions defined as ''stutters'' and ''stammers'' (Brown et al., 1996). Based on the analysis of the heptad repeat architecture, helical pitch and interhelical distances, we identify three distinct regions in the Ndel1 coiled-coil domain (Figure 1A). Regions I and II, separated by a stutter, together encompass residues 9–99, with five and seven complete heptads, respectively. Within that fragment, the two α helices form a tightly associated parallel coiled coil. Residues 100–106, while retaining an α-helical structure, contain a noncanonical sequence with no apparent heptad. Downstream of Ile107, the heptad repeats resume. We refer to the C-terminal fragment starting at residue 100 as Region III. This region forms an antiparallel four-helix bundle, which mediates the tail-to-tail

Table 1. Crystallographic Data

Data Collection				
	$Ndel1^{8–192}$			
Nominal λ (Å)	0.97928 (peak)	0.97945 (infl.)	0.97175 (remote)	1.54178 (CuKα)
Resolution	2.25	2.25	2.25	2.3
Total reflections	82,199	76,452	62,469	98,985
Unique reflections	40,587	37,442	34,338	21,413
Completeness[a]	87.9 (47.0)	79.6 (30.8)	73.3 (22.8)	96.4 (92.7)
R_{merge} (%)[b]	4.7 (18.1)	4.2 (26.1)	3.8 (31.8)	6.8 (38.7)
I/σ(I)	11.8 (3.6)	16.1 (2.6)	15.1 (2.1)	26.9 (3.0)
	$Ndel1^{58–169}$			
Nominal λ (Å)	0.97955 (peak)	0.97975 (infl.)	0.97565 (remote)	0.93300 (native)
Resolution	3.00	3.00	3.00	2.1
Total reflections	68,323	69,376	69,725	300,363
Unique reflections	9,092	9,207	9,303	26,088
Completeness	99.9 (100)[a]	100.0 (100.0)	100.0 (100.0)	99.8 (100.0)
R_{merge} (%)	5.1 (8.0)	4.6 (10.3)	5.5 (18.1)	7.5 (31.1)
I/σ(I)	9.1 (7.9)	8.9 (6.7)	6.4 (4.5)	4.9 (2.2)
Refinement				
	$Ndel1^{8–192}$ (CuKα)		$Ndel1^{58–169}$ (native)	
Model	325 aa (2671 atoms)		444 aa (3700 atoms) +125 waters	
Resolution	40–2.3		18–2.1	
Working/test sets	20,269/1,172		24,984/1,074	
R^c/R_{free} (%)	25.3/29.0		23.3/31.0	
Bond(Å)/angle(°) rms	0.011/2.37		0.026/1.92	
Ramachadran plot				
Most favored regions (%)	99.4		100.0	
Additional allowed regions (%)	0.6			

[a] The numbers in parentheses describe the relevant value for the last resolution shell, i.e., 2.33–2.25 Å for $Ndel1^{8–192}$, 3.16–3.0 Å for $Ndel1^{58–169}$ MAD data, and 2.17–2.10 for native $Ndel1^{58–169}$.
[b] $R_{merge} = \sum | I_i - < I > |/\sum I$ where I_i is the intensity of the ith observation, and $< I >$ is the mean intensity.
[c] $R = \sum||F_{obs}| - |F_{calc}||/\sum|F_{obs}|$, crystallographic R factor, and $R_{free} = \sum||F_{obs}| - |F_{calc}||/\sum|F_{obs}|$ where all reflections belong to a test set of randomly selected data.

interaction between the two Ndel1 parallel dimers (Figures 1A and 1B).

The homotetrameric association, evident in the crystal structures, is inconsistent with the established dimeric nature of Ndel1 in solution (Tarricone et al., 2004). This suggested to us that one of the intimate interfaces seen in the crystal structure, i.e., either the parallel interface between residues at the N terminus or the antiparallel bundle in the C-terminal portion, could in fact represent close crystal packing and not the biologically relevant interaction. To be in a better position to interpret the crystallographic data, we first investigated the nature of the oligomeric association of the Ndel1 coiled coil in solution.

The Oligomeric State of Ndel1 in Solution

To check if the Ndel1 coiled coil forms exclusively dimers in solution, we used analytical ultracentrifugation. The equilibrium absorbance profiles of three samples, i.e., $Ndel1^{8–192}$, $Ndel1^{8–99}$, and $Ndel1^{88–192}$ in 150 mM NaCl, were fitted to a single-species, monomer-dimer, or monomer-tetramer model (data not shown). The data for $Ndel1^{8–99}$ fitted well to a single-species model with a molecular weight of 23,749 ± 532 Da (based on three measurements), consistent with a dimer. The data from three experiments with $Ndel1^{8–192}$ also fitted to a single-species model with a molecular weight of 43,246 ± 1214 Da, again consistent with a dimer. A tetrameric species was not detectable in 150 mM NaCl solution. However, in an

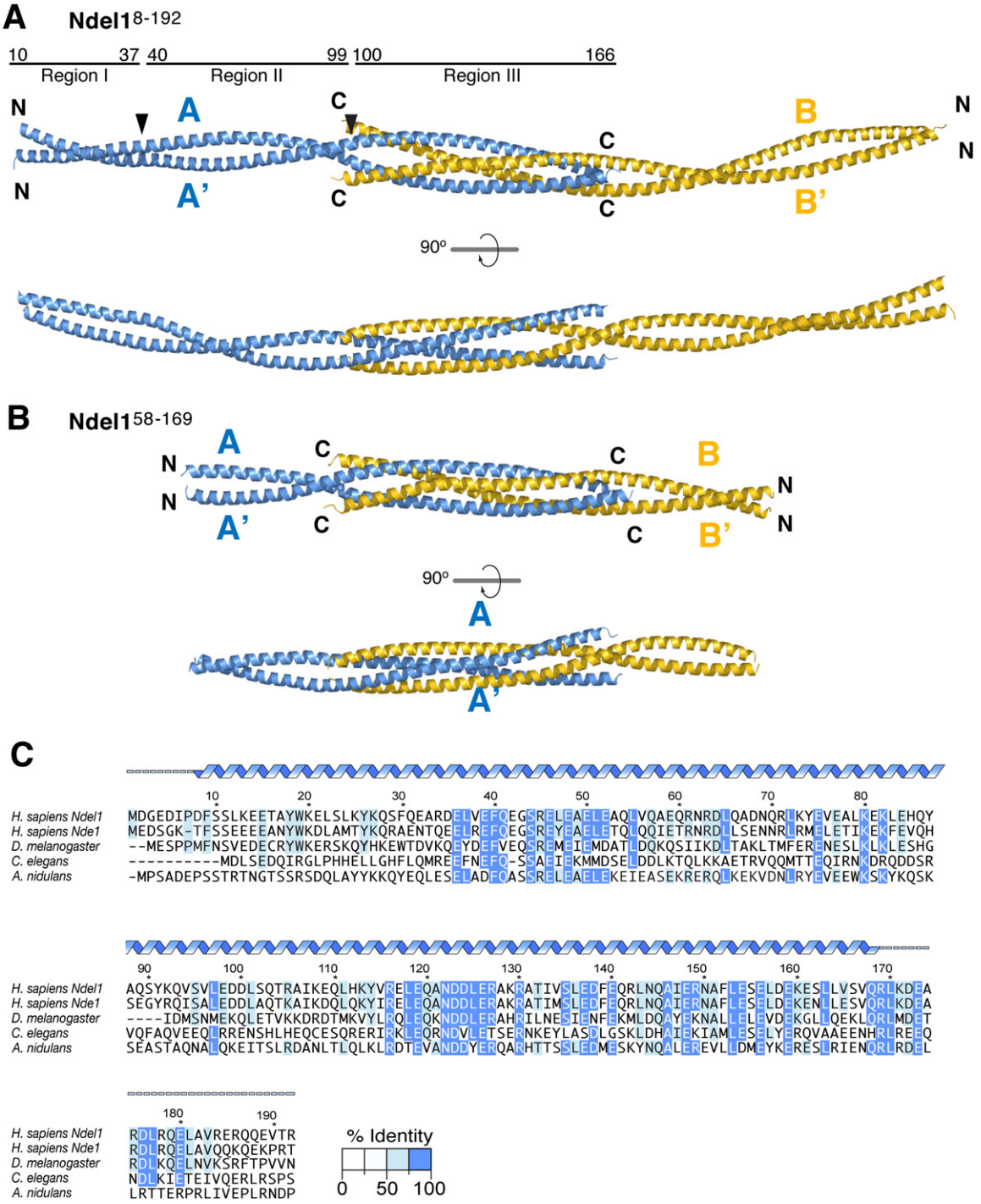

Figure 1. The Structure and Sequence Alignment of the Coiled-Coil Domain of Ndel1

(A) Two orthogonal views of the crystal structure of Ndel1$^{8–192}$. Note that the yellow B/B′ dimer in the Ndel1$^{8–192}$ is related to the blue A/A′ dimer by crystallographic two-fold symmetry. For detailed description of the three regions, see text.

(B) Two orthogonal views of the crystal structure of Ndel1$^{58–169}$. The entire homotetramer, consisting of the blue A/A′ dimer and the yellow B/B′ dimer, occupies an asymmetric unit.

(C) Structure-guided alignment of the amino acid sequences of the human Ndel1 and Nde1 proteins, together with selected sequences of Ndel1 from other species. The degree of conservation was calculated based on an alignment of 14 Nde1 and Ndel1 sequences in different organisms. The program PYMOL (http://www.pymol.org/) was used in this and subsequent figures to generate the molecular diagrams.

experiment carried out in 1 M NaCl, Ndel1$^{8–192}$ absorbance profile data yielded a weight-average molecular weight of 48,905 Da, which could not be fitted to a single-species model, but instead fitted better to a dimer-tetramer model, with 13% tetramer content (data not shown). The data for Ndel1$^{88–192}$ from two separate experiments gave a weighted average molecular weight also higher than that of the monomer but fitted to a monomer-tetramer model with a tetramerization constant K_T in the 10^{11}–10^{12} M^{-3} range ($K_T = [T]/[M]^4$, where [T] and [M] are molar concentrations of the tetrameric and monomeric species, respectively). These data confirmed previous observations that a dimer is the predominant species for the Ndel1 coiled coil in solution but also revealed that—at least under some conditions—the fragment encompassing primarily region III has a tendency to form low-affinity tetramers.

We then asked what type of dimer is prevalent in solution, i.e., parallel or antiparallel. To resolve this issue, we used site-directed spin labeling (SDSL) (Fanucci and Cafiso, 2006). We generated two single-site, spin-labeled mutants of the Ndel1$^{8–192}$ fragment, i.e., Q120C^{R1} and A151C^{R1}, where R1 denotes the methanethiosulfonate, or MTSL, label. We then analyzed the distances between the two spin labels in the Q120C^{R1} and A151C^{R1} homodimers. Assuming that the paramagnetic center of the nitroxide moiety is located approximately 6.7 Å from the center of the α-helix (Rabenstein and Shin, 1995), the distance between two labels on identical residues in a canonical parallel two-stranded coiled coil with an interhelical distance of ~10 Å, should be ~24 Å. In contrast, in an antiparallel dimer, the spin labels attached to A151^{CR1} would be expected to be >55 Å apart, while those bound to Q120^{CR1} should be >32 Å apart. We measured the distances using double electron-electron resonance (DEER), which allows for echo measurements of up to 80 Å (Fanucci and Cafiso, 2006). The distances between the labels in both Q120C^{R1} and A151C^{R1} were consistent with a parallel, tightly wound coiled coil (Figure 2).

Finally, to better understand the dynamics of the Ndel1 coiled coil, we used far UV circular dichroism (CD) spectroscopy. We used samples of Ndel1$^{8–192}$, Ndel1$^{8–99}$, Ndel1$^{88–192}$, and Ndel1$^{102–174}$ to record spectra in benign buffer conditions and in 50% (v/v) trifluoroethanol (TFE), which disrupts the coiled coil and stabilizes isolated α helices. Under benign conditions, all samples with the exception of Ndel1$^{102–174}$ showed spectra characteristic of α-helical proteins with double minima at 208 and 222 nm (Figure 3B and Table 2). Based on the comparison of observed and calculated molar ellipticities at 222 nm, we find that both Ndel1$^{8–192}$ and Ndel1$^{8–99}$ are fully helical. In contrast, Ndel1$^{88–192}$ is ~60% helical, while Ndel1$^{102–174}$ shows only marginal helical content. In 50% TFE, Ndel1$^{88–192}$ recovers most of its propensity to form a helix, while Ndel1$^{102–174}$ does so to a limited degree only. Further, under benign conditions, the ratio of ellipticities (222/208 nm) was significantly greater than 1.0 for Ndel1$^{8–99}$ and Ndel1$^{8–192}$, suggesting that both form predominantly coiled coils. In contrast, for Ndel1$^{88–192}$ this ratio was ~0.9, consistent with weaker interaction between the α helices.

During thermal denaturation, all samples denature reversibly and cooperatively (Figure 3C). The Ndel1$^{8–99}$ and Ndel1$^{8–192}$ fragments melt at the same temperature (T_m) of ~50°C. In contrast, the Ndel1$^{88–192}$ fragment has distinctly lower stability with T_m ~31°C, while the Ndel$^{102–174}$ fragment has a transition midpoint temperature at ~23°C.

Thus, based on the DEER and CD experiments, we conclude that the Ndel1 coiled coil forms predominantly parallel dimers in solution, stabilized by regions I and II, which together comprise the dimerization domain. The four-helix bundle that is formed in the crystals by region III is clearly a reflection of this region's instability and tendency to unwind, leading to higher oligomeric forms that may—or may not—represent physiologically relevant species. As we discuss below, the sequence and structure of region III further rationalize this observation.

The Structure of the Dimerization Domain, Regions I and II

Within the dimerization domain we identified a total of 13 ***a–g*** heptads between Phe9 and Val96. Twelve are complete, while residues Leu37 to Phe40 constitute an incomplete ***abcd*** heptad or stutter, which separates region I from region II.

Within the five contiguous heptads of region I, the two α helices form a tight supercoil with an average pitch of 143 Å and an interhelical distance of ~8.4 Å. These values are lower than expected for a canonical coiled coil, where the pitch is ~180 Å and the interhelical distance ~9.6 Å (O'Shea et al., 1991). The buried interface between the α helices is formed by alternating layers of ***aa′*** and ***dd′*** positions, typical for parallel coils: layers ***aa′*** are formed by Phe9, Thr16, Ser23, Phe30, and Leu37, while layers ***dd′*** are formed by residues Leu12, Trp19, Tyr26, Ala33, and Phe40 (Figure 4). There is conspicuous absence among the ***d*** residues of the most stabilizing amino acids such as Leu, Met, and Ile, (Tripet et al., 2000), but instead we note a preponderance of aromatic side chains. The ***g*** position contains only two negatively charged residues, resulting in one potential interhelical H-bond (Glu15^{A}-Lys20$^{A′}$). The ***e*** position contains exclusively positively charged residues, while the ***f*** position is mostly negative, conferring a unique charge distribution on this fragment.

After the stutter following Glu39, at the beginning of region II, the helices abruptly move away from each other and assume a virtually parallel course with the pitch increasing locally to a staggering 1400 Å at Gly43. Local unwinding is often seen as a compensatory effect alleviating the effect of stutters (Brown et al., 1996; Strelkov and Burkhard, 2002). Immediately downstream, the coiled coil resumes a more canonical stereochemistry with the average pitch ~150 Å and the interhelical distance in the 9.6–10.2 Å range. At Val94, the pitch of the coiled coil is reduced again to 110 Å, with the interhelical distance of about 10.4 Å. Region II includes seven complete heptads (Figure 4). Here, the interface ***aa′*** layers are formed by

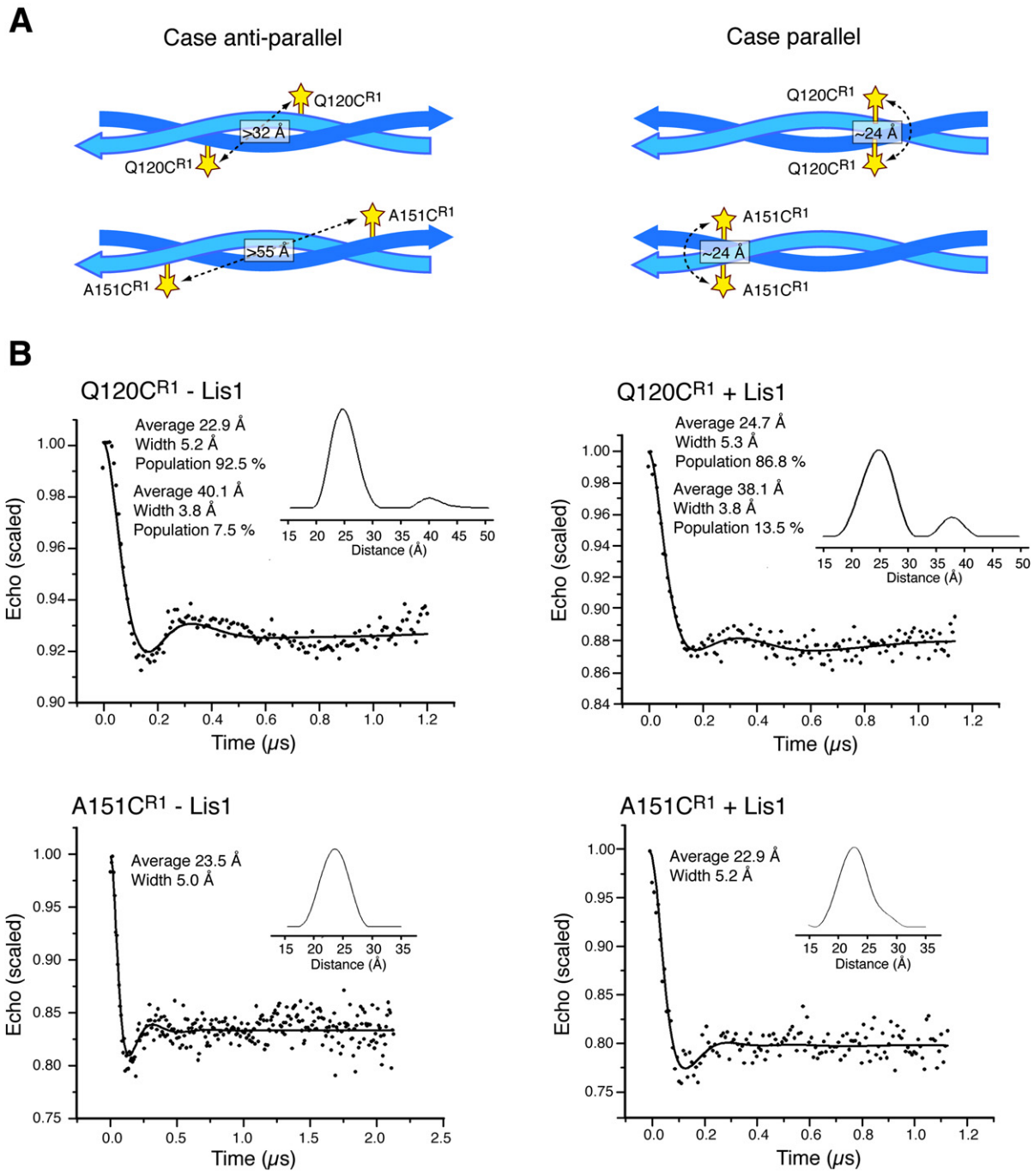

Figure 2. The Results of DEER Experiments

(A) A schematic representation showing the hypothetical mutual disposition of Q120C^{R1} and A151C^{R1} in parallel and antiparallel coiled coil.

(B) DEER spectra for Q120C^{R1} and A151C^{R1}, in isolation (left panels) and in the presence of Lis1 (right panels). The Q120C^{R1} mutant shows a minor component with an interlabel distance of ~40 Å, which we interpret as evidence of an alternative conformation of the label.

Glu48, Leu55, Asn62, Asn69, Val76, Leu83, Ser90, and Leu97. The hydrophobic residues are key to the stability but—interestingly—the central location is occupied by two consecutive asparagines, which are known to play a significant role in this position in enforcing two-stranded as opposed to higher oligomeric states oligomerization (Gonzalez et al., 1996a, 1996b, 1996c). The ***dd′*** layer is generated by Ser44, Leu51, Ala58, Leu65, Leu72, Leu79, Gln86, Gln93. This layer contains five leucines, which confer maximum stability on the coiled coil. The ***c***, ***g***, and ***e*** positions contain a mixture of polar and charged residues, which make up several salt bridges. One such interhelical

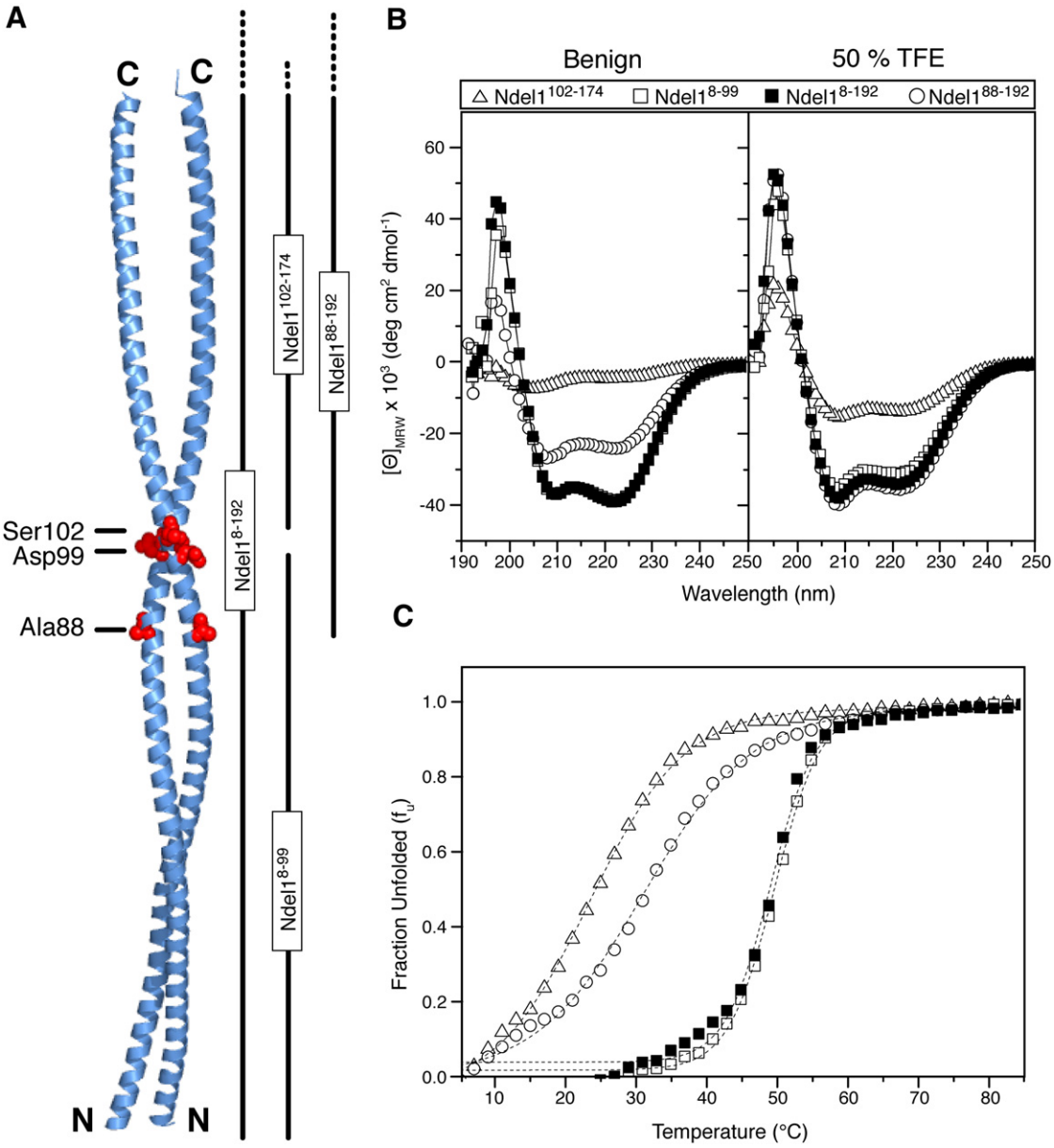

Figure 3. CD Spectroscopy of the Coiled-Coil Domain of Ndel

(A) A diagrammatic representation of the constructs used in the analysis.

(B) Ultraviolet CD spectra recorded for benign buffer conditions and in 50% TFE.

(C) Thermal denaturation of the different constructs monitored by ellipticity change at 222 nm.

bridge is formed by Glu59^{A} and Arg61$^{A'}$, while an intrahelical salt zipper connects Asp68^{A}, Arg71^{A}, and Glu75^{A}, with the latter forming an additional interhelical bridge with Lys80$^{A'}$.

In the Ndel1$^{58–169}$ structure, the corresponding fragment of the dimerization domain overlaps well with that in the Ndel1$^{8–192}$ structure with an rms difference for main chain atoms of ~1 Å. The mean interhelical distance is ~10 Å with the supercoil pitch of ~140 Å, in good agreement with the Ndel1$^{8–192}$ structure.

The Transition Peptide and the Antiparallel Four-Helix Bundle, Region III

Region II terminates at Asp99. Leu97 occupies an ***a*** site expected for a hydrophobic amino acid, but the downstream sequence, EDDLSQTRA, is quite unusual and breaks the canonical 3:4 hydrophobic repeat. Coil prediction program, COILS (Lupas, 1997; Lupas et al., 1991), shows here a discontinuity, particularly pronounced when a 14 residue sliding window is used. The first amino acid to violate the repeat in this sequence is Asp100,

Table 2. Circular Dichroism of Ndel1 Fragments

Fragments	$[\Theta]_{222}$[a]	% Helix #1	% Helix #2	$[\Theta]_{222}/[\Theta]_{208}$	$T_{1/2}$[b] (°C)
Ndel1 (102–174)	−3,316	9	9	0.63	23.5
Ndel1 (88–192)	−23,116	63	60	0.91	31.2
Ndel1 (8–99)	−37,450	100	98	1.05	49.7
Ndel1 (8–192)	−37,990	100	97	1.07	49.1

[a] Mean residue molar ellipticities at 222 nm (deg cm^2 $dmol^{-1}$) were measured at 25°C in benign buffer (150 mM NaCl, 50 mM sodium phosphate buffer [pH 7.0]) and in equal volumes of benign buffer and 2,2,2-trifluoroethanol (TFE). The predicted molar ellipticity for a completely of α-helical peptide was calculated with two formulas: $[\Theta]_{theoretical} = 37{,}400 \times (1 - 2.5/N)$, and $[\Theta]_{theoretical} = 40{,}000 \times (1 - 4.6/N)$, where N is the number of residues in the polypeptide chain. The helical fraction at 25°C was calculated from $[\Theta]_{222}$ as the $[\Theta]_{observed}$ divided by the $[\Theta]_{theoretical}$.

[b] $T_{1/2}$ is the transition midpoint temperature at which there is a 50% decrease in molar ellipticity, $[\Theta]_{222}$, compared with the fully folded protein as determined by CD at 5°C.

which occurs in the normal ***d*** position. Aspartates are typically disfavored at the ***d*** position (Tripet et al., 2000), and in both Ndel1 crystal structures, Asp100 are in a near steric clash, protruding into the coiled-coil interface. In the electron density maps, the two carboxyl groups are within 3 Å of each other within the otherwise hydrophobic core, suggesting that one of them might be protonated.

A distinct structural change is clearly seen in both our crystal structures in this region. The two α helices, which up to this point are tightly supercoiled with an interhelical distance of ~10 Å, move away from each other, so that the distance is ~13 Å at Thr104. As they separate, the α helices continue as a left-handed supercoil, but with a pitch that gradually increases from 101 Å at Asp100 to ~400 Å at Asn122. The unwinding of the two α helices makes room for the symmetry-related dimer to interlock in the form of the antiparallel four-helix bundle, in which each helix interacts with both antiparallel counterparts via independent interfaces, i.e., the A/B and A/B′ interfaces. The assignment of the heptads in region III is not trivial. In general terms, the heptad repeat resumes at Ile107 as position ***d*** and continues over nine heptads, with one stutter, Thr132, Ile133, Val134, Ser135. This is the only scheme that accommodates the remaining hydrophobic residues in the ***a*** and ***d*** positions, with few outliers (Ile147, Phe152, Leu163), one in the ***e*** and two in the ***g*** positions, respectively (Figure 4). Thus, the packing of the four helix bundle places the ***a*** and ***d*** positions in its core, in a canonical fashion. There are electrostatic zippers across the two distinct antiparallel interfaces involving either the ***e*** or ***b*** residues within one interface and the ***g*** residues within the other (Figure 4B). Across the A/B (and A′/B′) interface, $Glu140^B$ interacts with $Lys129^A$ (both ***e*** residues), $Asn144^B$ (***b***) with $Asn122^A$ (***e***), $Lys108^A$ (***e***) with $Asp158^B$ (***b***), $Glu161^B$ (***e***) with $Arg105^A$ (within the transition peptide), and $Glu154^B$ (***e***) with $His112^A$ (***b***). Across the A/B′ (and A′/B) interface, an electrostatic zipper is made up by interdigitating ***g*** residues: $D124^A$-$R142^{B'}$-$E117^A$-$R149^{B'}$-$Q110^A$.

There are some small differences in the degree of compactness of this bundle between the two crystal structures. The cross-section of the $Ndel1^{8–192}$ bundle is rectangular at its midpoint, with two pairs of antiparallel strands, AB and A′B′, closer together than the AB′ and A′B pairs (i.e., ~11 Å versus ~14 Å). In the $Ndel1^{58–169}$ structure, the cross-section is closer to a square. We attribute these small differences primarily to crystal contacts exerting lateral forces on the helices.

Interaction with Lis1

It has been shown previously that $Ndel1^{85–154}$ is capable of binding Lis1, but $Ndel1^{1–84}$ is not (Tarricone et al., 2004). The dissociation constant K_D for the interaction between homodimeric Ndel1 and homodimeric Lis1 was shown to be in the sub-μM range, as measured by titration microcalorimetry (Tarricone et al., 2004). Additional pull-down assays confirmed that recombinant full-length Lis1 binds to both $Ndel1^{8–192}$ (data not shown) and $Ndel1^{58–169}$ (Figure 5) but not to the isolated dimerization domain of Ndel1 (residues 8–99, data not shown).

To better characterize the Lis1-interaction epitope, we carried out further deletion analysis of Ndel1 and a limited scanning alanine mutagenesis of a number of charged and hydrophobic residues on the solvent-exposed face of region III of the $Ndel1^{58–169}$ fragment. $Ndel1^{1–153}$ binds to Lis1, as does $Ndel1^{103–169}$, while $Ndel1^{1–148}$ does not bind Lis1 (Figure 5A). We conclude that residues 103–153 contain the minimal Lis1-binding domain of Ndel1. Among the single-site mutants, E119A and R130A showed no affinity for Lis1, and the D123A mutant showed decreased affinity (Figure 5B). All three residues are conserved among Ndel1 homologs.

To complement the binding studies, we used site-directed spin labeling (SDSL) (Fanucci and Cafiso, 2006). In addition to the previously generated, spin-labeled $Q120C^{R1}$ and $A151C^{R1}$ mutants of the $Ndel1^{8–192}$ fragment, we prepared $S102C^{R1}$, $R130C^{R1}$, $I133C^{R1}$, $Q141C^{R1}$, and $D158C^{R1}$. All bound Lis1 in pull-down assays, with the exception of $R130C^{R1}$ (Figure 6). Continuous wave (CW) EPR spectra were then recorded in the presence and absence of Lis1. Such spectra allow for identification of substantial decrease in the mobility of the label when it is sequestered at or near an interface with an interacting protein. In agreement with the deletion studies, we observed that the $S102C^{R1}$ and $D158C^{R1}$ spectra were virtually unperturbed in the presence of Lis1, suggesting that these residues lie outside the Lis1-binding domain. In contrast, both $Q120C^{R1}$ and $A151C^{R1}$ showed strong ordering, while $I133C^{R1}$ and $Q141C^{R1}$ displayed smaller effects (Figure 6).

Given that we have already established that in solution region III forms primarily a dimeric parallel coiled coil, albeit unstable, we next asked if in complex with Lis1 the two α helices maintain this conformation. We therefore

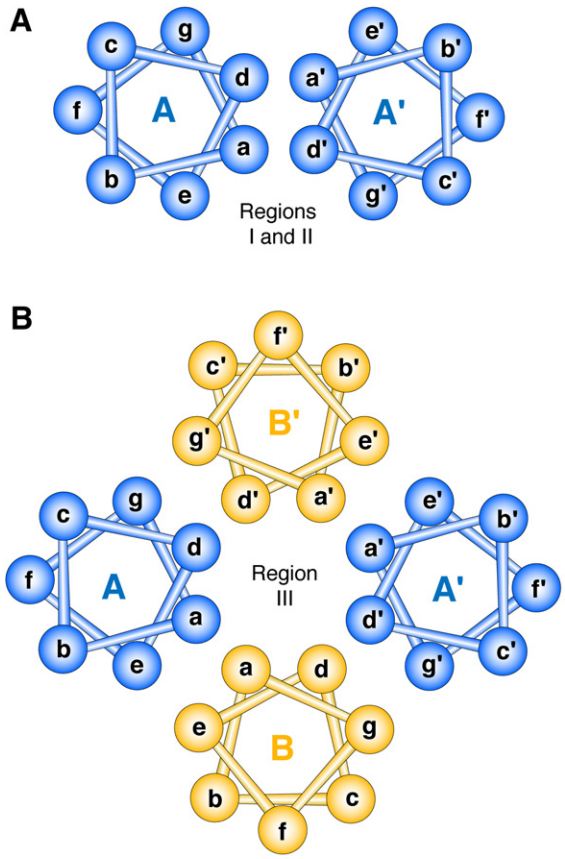

C

Heptad repeats: Region I

a	*b*	*c*	*d*	*e*	*f*	*g*
F9	S10	S11	L12	K13	E14	E15
T16	A17	Y18	W19	K20	E21	L22
S23	L24	K25	Y26	K27	Q28	S29
F30	Q31	E32	A33	R34	D35	E36
L37	V38	E39	F40			

Heptad repeats: Region II

a	*b*	*c*	*d*	*e*	*f*	*g*
			S44	R45	E46	L47
E48	A49	E50	L51	E52	A53	Q54
L55	V56	Q57	A58	E59	Q60	S29
N62	R63	D64	L65	Q66	A67	D68
N69	Q70	R71	L72	K73	Y74	E75
V76	E77	A78	L79	K80	E81	K82
L83	E84	H85	Q86	Y87	A88	Q89
S90	Y91	K92	Q93	V94	S95	V96
L97	E98	D99				

Heptad repeats: Region III

a	*b*	*c*	*d*	*e*	*f*	*g*
			I107	K108	E109	Q110
L111	H112	K113	Y114	V115	R116	E117
L118	E119	Q120	A121	N122	D123	D124
L125	E126	R127	A128	K129	R130	A131
T132	I133	V134	S135			
L136	E137	D138	F139	E140	Q141	R142
L143	N144	K145	A146	I147	E148	R149
N150	A151	F152	L153	E154	S155	E156
L157	D158	E159	K160	E161	S162	L163
L164	V165	S166				

Figure 4. Helical Wheels for Regions I, II, and III

(A) A diagrammatic representation of the parallel coiled coil as observed for regions I and II.

(B) A diagrammatic representation of the four helix bundle made up by region III; the blue helices are seen along the axes from the N to C termini, the yellow helices are seen in the opposite direction.

(C) The assignment of heptad positions in all three regions of the coiled coil.

repeated the DEER experiments with the Q120C^{R1} and A151C^{R1} variants, but in the present of excess of Lis1. The distances between the labels were once more consistent with a parallel coiled coil, showing Ndel1 does not undergo any structural rearrangement upon binding Lis1 and retains the overall architecture of a parallel coiled coil (Figure 2).

Previously published data strongly suggest that Ndel1 does not bind isolated β-propeller domains of Lis1, and its interaction with the N-terminal domain of Lis1 is at best very weak (Niethammer et al., 2000; Sasaki et al., 2000; Tarricone et al., 2004). Our attempts to detect interactions between the Ndel1$^{8–192}$ fragment and the ^{15}N labeled N-Lis1 domain (residues 1–86) by NMR have failed. We therefore conclude that the interaction of Ndel1 with Lis1 is mediated primarily by the β-propellers but that it requires the presence of intact dimers of both proteins. We note that the dimensions of the Lis1 β-propellers would in principle allow this domain to interact with a segment of the Ndel1 coiled coil between residues 119 and 151. If we assume that this fragment retains the approximate overall pitch seen in the crystal structures, residues Glu119 and Gln120 (both involved in the interaction as indicated by pull-down assays and EPR, respectively) should be located on one face of the coiled coil, while Arg130, Ile133, and Ala151 make up a second epitope on the opposite face of the coiled coil. This implies that each of the two Lis1 β-propellers in the Lis1 dimer interact cooperatively with both Ndel1 α helices, as shown diagrammatically in Figure 7.

Conclusions

Using a range of complementary and synergistic biophysical methods, we characterized the structure and dynamics of the Ndel1 coiled coil, both in isolation and in a complex with Lis1. We showed that the coiled coil domain of Ndel1 is a complex structure with three distinct regions. Regions I and II—encompassing together the N-terminal portion up to residue Val 96 and separated by an intervening stutter—form a tightly associated, highly stable canonical parallel dimer, with a classical 3:4 hydrophobic heptad repeat. Region III, which is separated from the dimerization domain by an unusual sequence lacking the canonical heptad repeat, is unstable in isolation and

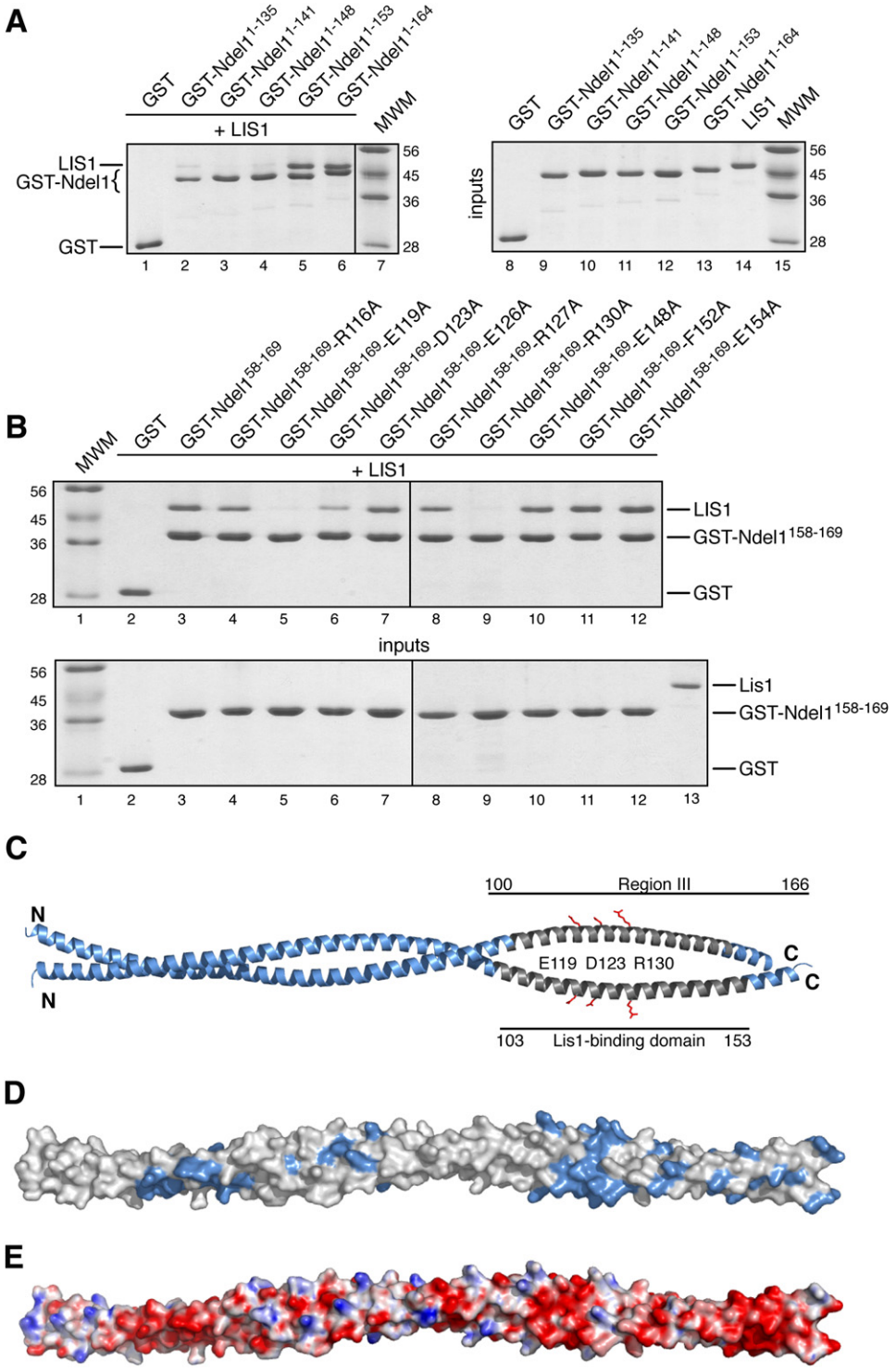

Figure 5. Probing Ndel1/Lis1 Interactions

(A) Left panel: deletion mapping of the Lis1-binding region of Ndel1. The indicated deletion constructs of GST-Ndel1, immobilized on GSH beads, were incubated with purified Lis1. Lis1 bound to GST-Ndel1$^{1-153}$ (lane 5) or GST-Ndel1$^{1-164}$ (lane 6) but was unable to bind to GST or to shorter Ndel1 constructs (lanes 1–4). Right panel: the input proteins used in the binding assay.

(B) Upper panel: analysis of the effects of point mutations on the Ndel1-Lis1 interaction. The indicated GST-Ndel1 mutants were immobilized on GSH beads and incubated with Lis1. Two mutants (E119A and R130A, lanes 5 and 9) were unable to bind Lis1. D123A showed decreased binding. The gel is a representative example of at least five assays. Bottom panel: the input proteins used in the binding assay.

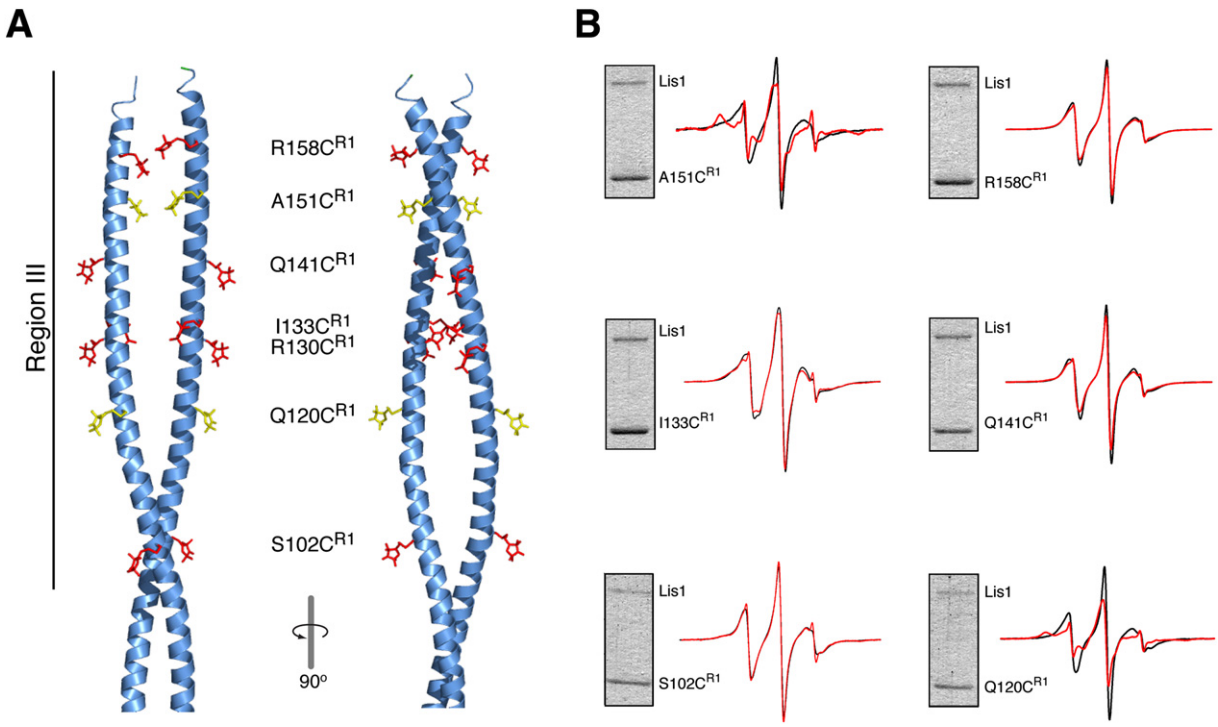

Figure 6. Site-Directed Spin Labeling and CW-EPR Experiments

(A) Two orthogonal views of region III showing the locations of spin labels based on the conformation of the R1-modified cysteines as observed in lysozyme (Langen et al., 2000). The two labeled residues shown to be most sensitive to binding, Cys151^{R1} and Cys120^{R1}, are shown in yellow.

(B) Continuous-wave EPR spectra are shown for each mutant measured both in isolation (black) and in the presence of Lis1 (red). The panels on the right visualize the results of pull-down assays demonstrating that the spin-labeled mutants retain the ability to bind to Lis1. Proteins are visualized by Coomassie stain in SDS-PAGE.

shows a tendency to unwind under benign conditions. Nonetheless, in solution, a parallel dimer is the prevalent species. In contrast, the crystal structure shows Region III engaged in an antiparallel four helix bundle, generated by a tail-to-tail association of Ndel1 coiled coils. This quaternary arrangement is conserved in crystal structures of two different constructs in two different crystal forms, suggesting that it is formed in solution and selectively crystallized. The propensity of isolated region III to form tetramers had been confirmed by ultracentrifugation, lending further support to the notion that the tail-to-tail structure is not purely a crystallization artifact.

An important question is if the observed, low affinity tetrameric interaction is biologically relevant. Although in the absence of any experimental evidence we can only speculate, nonetheless several observations suggest that such a hypothesis should be investigated.

We note, for example, that although region III has an apolar face made up of the ***a*** and ***d*** residues, thus mostly conforming to the 3:4 motif, the distribution of hydrophobic residues between the ***d*** and ***a*** positions is not favorable for a two-stranded parallel coiled coil. It is well established that the packing interactions depend on the stereochemistry of residues in the ***a*** and ***d*** positions. In a parallel two-stranded coiled coil, the ***a*** position favors β-branched side chains, while ***d*** layers favor the unbranched leucine (Lupas and Gruber, 2005). The preferences are reversed in a parallel four-stranded coiled coil, and in antiparallel dimmers, the alternating ***ad′*** layers lead to mixed geometries. In fact, leucine has been experimentally shown to be the most stabilizing aliphatic amino acid in the ***d*** position in parallel coiled coil (Moitra et al., 1997; Tripet et al., 2000). In contrast, the presence of Leu in the ***a*** position is less favorable and is likely to affect the oligomerization state, leading to a trimeric species (Wagschal et al., 1999). In region III of Ndel1, the heptad motif shows a preponderance of leucines in the ***a*** position—seven out of nine heptads have that residue—while in the ***d*** position, we find a mixture of amino acids with three alanines, a valine, an isoleucine, a phenylalanine, a tyrosine, and one leucine (Figure 4). Thus, the sequence analysis alone suggests that the parallel coil in this region should be disfavored in the absence of additional stabilizing factors, such as the dimerization domain upstream, or specific interacting proteins. The

(C) A diagrammatic representation of the Ndel1$^{8–192}$ parallel dimer with the residues E119, D123, and R130 shown for clarity; the dimer is depicted as observed in the crystal structure and is not identical to the species in solution.

(D) Conservation pattern along the length of the coiled-coil domain: the absolutely conserved residues are blue.

(E) Charge distribution: red and blue colors denote negatively and positively charged amino acids, respectively.

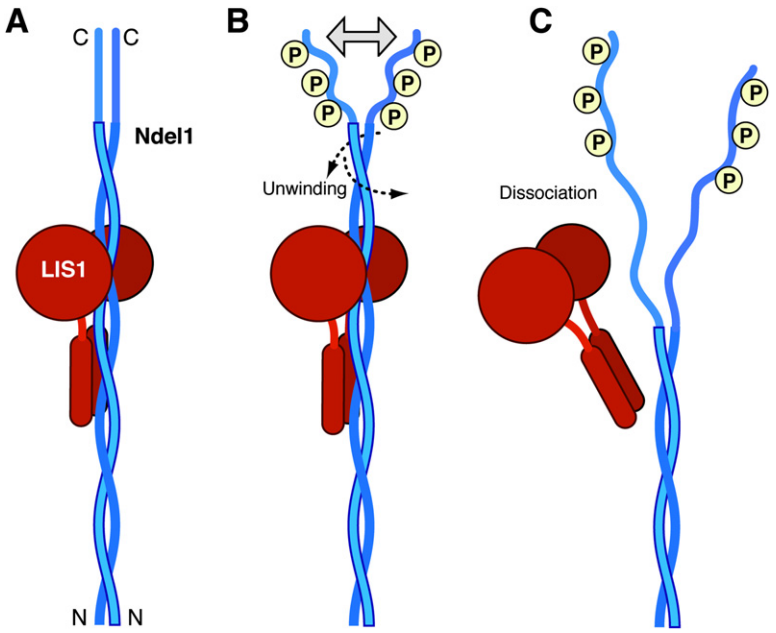

Figure 7. A Model of Phosphorylation-Dependent Negative Regulation of the Lis1-Ndel1 Interaction

(A) A hypothetical complex between the Lis1 homodimer and the Ndel1 homodimer, as inferred from the experimental data presented in this paper.

(B) The phosphorylation of the C-terminal domain of Ndel1 initiates unwinding of region III.

(C) As a result of destabilization of region III, possibly through interaction of phosphorylated sites by other proteins, including 14-3-3, Lis1 dissociates from Ndel1.

circular dichroism experiments that we report in this paper fully confirm this notion.

Interestingly, it is region III, or rather a segment within this region encompassing approximately residues 103–153, that is responsible for the biologically important interaction with Lis1. This entire fragment has nearly identical sequences in both Ndel1 and Nde1, with only five very conservative substitutions, i.e., K105R, E109D, H112Q, V115I, V134M. Moreover, it is also the most evolutionarily conserved fragment of Ndel1. Such high degree of conservation may reflect evolutionary constraints acting not only on the Lis1-interacting surfaces but also on the unusual heptad pattern in region III.

Since region III is very unstable, its structure may be easily modulated by any of the proteins shown to interact with the C-terminal domain of Ndel1, downstream of the coiled coil, often in phosphorylation-dependent manner. The C-terminal domain contains numerous phosphorylation motifs, and it has been shown that Cdk5, Cdc2, Cdk1, and Aurora A indeed use Ndel1 as substrate (Mori et al., 2007; Niethammer et al., 2000; Toyo-Oka et al., 2005; Toyo-oka et al., 2003; Yan et al., 2003), leading to the recruitment of other proteins to the complex. It is tempting to speculate, that at least some of these interactions may results in destabilization of region III and unwinding of the coiled coil with concomitant loss of affinity for Lis1 (Figure 7). To our knowledge, such negative regulation of Ndel1 and of its interaction with Lis1 has never been considered. We are currently testing these hypotheses experimentally.

EXPERIMENTAL PROCEDURES

Cloning, Expression, and Purification

Fragments of murine Ndel1 (which is identical with respect to the amino acid sequence to the product of the human ortholog) including Ndel1$^{8–192}$, Ndel1$^{8–99}$, Ndel1$^{88–192}$, and Ndel1$^{102–174}$ were expressed in *E. coli* BL21(DE3) RIPL cells (Stratagene, Inc.) in fusion with a hexa-His-tag by using the pHisUni1 expression vector (Sheffield et al., 1999) and purified by standard methods. To generate Se-labeled samples for crystallography, Leu 24 and Val 134 were mutated to Met, and the protein was expressed in *E. coli* B834 (DE3). The human Ndel1$^{58–169}$ fragment was overexpressed and purified as described elsewhere (Tarricone et al., 2004). For the MAD experiment, residues Val134 and Leu153 were mutated to methionines. Lis1 was expressed in insect cells as described previously (Tarricone et al., 2004). Site directed mutagenesis was carried out with QuikChange (Stratagene).

Crystallization, Data Collection, and Structure Determination

Crystals of Ndel$^{58–169}$ ($P2_1$, a = 46.4 Å, b = 73.2 Å, c = 69.0 Å, β = 105.4) grew in one week by vapor diffusion at 20°C from equal volumes of 20 mg/ml protein solution and a reservoir buffer containing 4% PEG 8000, 50 mM sodium phosphate (pH 6.8), and 100 mM NaCl. Crystals were harvested in reservoir buffer and cryo-protected by incubation in reservoir buffer supplemented with 17% PEG 400. SeMet-containing crystals of the (V134, L153)→M mutant were obtained by microseeding with wild-type Ndel1$^{58–169}$, with 5 mM DTT. X-ray data were collected at beamlines ID14-1, ID23-1, and ID29 at the ESRF, Grenoble (Table 1). Before cryoprotection, crystals were oxidized with H_2O_2. This resulted in a 20% increase in the anomalous signal as judged by fluorescence scans. X-ray diffraction data were integrated with MOSFLM and reduced with SCALA (CCP4, 1994). The Se-substructure was identified with SHELXD (Schneider and Sheldrick, 2002), phasing was done with SHARP 2.0 (Bricogne et al., 2003), and the atomic model was built with ARP-wARP (Morris et al., 2003b) and refined with REFMAC (Murshudov et al., 1997).

Crystals of Ndel1$^{8–192\ (L24,V134)→Met}$ mutant (C2, a = 90.0 Å, b = 45.4 Å, c = 124.7 Å, β = 97.2°) were grown by using 18%–22% tert-butanol, 100 mM sodium citrate (pH 6.0), 10 mM $CoCl_2$, and 10 mM spermine as the precipitant solution. Before freezing, tert-butanol was exchanged for 30% MPD. MAD data were collected at the APS (Argonne National Laboratory), SERCAT beamline and processed with HKL2000 (Otwinowski and Minor, 1997) (Table 1). A high-quality data set was collected by using an Enraf-Nonius rotating anode source equipped with confocal mirrors and an r axis IV image plate system, and this set was used for the final refinement. The structure was phased using SOLVE (Terwilliger and Berendzen, 1999) with iterative model building and refinement in RESOLVE (Terwilliger, 2003) followed by extensive manual rebuilding with O (Jones et al., 1991) and COOT

(Emsley and Cowtan, 2004), with final refinement with REFMAC (Murshudov et al., 1997). The stereochemical analysis of the coiled coil was carried out with SOCKET (Walshaw and Woolfson, 2001) and TWISTER (Strelkov and Burkhard, 2002).

Analytical Ultracentrifugation

Sedimentation equilibrium experiments were performed with a Beckman Optima XL-I analytical ultracentrifuge by using absorbance optics. A Ti50 eight-hole rotor was used with six-sectored centerpieces. Samples of Ndel1$^{8–99}$, Ndel1$^{88–192}$, and Ndel1$^{8–192}$ (three concentrations of each with absorbances of 0.25, 0.50, and 0.75 at 280 nm) were spun at 24,000 rpm for 20–24 hr at 20°C. Absorbance scans at 280 nm were recorded every 2 hr. Equilibrium was assumed to have been reached when the difference between two consecutive absorbance profiles became zero. The meniscus-depletion method was used to determine absorbance offsets after overspeeding the samples at 40,000 rpm for 6 hr. Equilibrium absorbance profiles were analyzed with the Beckman XL-A/XL-I Analysis Software Version 5.0.

CD Spectropolarimetry

Circular dichroism (CD) spectra were recorded on an AVIV Model 215 CD spectropolarimeter (AVIV Instruments, Lakewood, NJ) equipped with a thermoelectric temperature control. Data were recorded from 190 to 250 nm in benign buffer (150 mM NaCl, 50 mM phosphate [pH 7.0]), and in buffer diluted 1:1 (v/v) with trifluoroethanol (TFE). Thermal melting temperatures (T_m) were determined by following the change in molar ellipticity at 222 nm in a 0.1 cm pathlength cell and a temperature increase rate of 1°C/min. The temperature range was 25°C–85°C for Ndel1$^{8–99}$ and Ndel1$^{8–192}$ and 5°C–85°C for Ndel1$^{88–192}$ and Ndel1$^{102–174}$. Ellipticity readings were normalized to the fraction of protein unfolded (f_u) by standard protocols.

EPR Measurements

The Ndel1 X→C mutants were mixed DTT at 4°C for 1 hr followed by size-exclusion chromatography and incubation with a 30-fold molar excess of spin label (1-oxyl-2, 2, 5, 5-tetramethyl-3-pyrroline-3-methyl) methanthiosulfonate (MTSL) at room temperature, overnight in the dark. Free spin label was removed by size-exclusion column on the Superdex 75 column (Amersham Pharmacia Biotech). The labeled proteins were concentrated with a centrifugal concentrator Microcone-10, Amicon. Continuous wave (CW) EPR spectroscopy was performed on a Varian E-line 102 series X-band spectrometer equipped with a loop-gap resonator (Medical Advances, Milwaukee, WI). Data were collected as described elsewhere (Xu et al., 2006). Four-pulse DEER measurements were performed with a Bruker Elexsys 580 spectrometer equipped with a 2-mm split-ring resonator under conditions of strong overcoupling (Q = 200) at ~80 K as described elsewhere (Xu et al., 2006). The distance distribution $P(r)$ was obtained by Tikhonov regularization, and the optimal regulation parameter was chosen from the L-curve computed in the DEERAnalysis 2006 package.

ACKNOWLEDGMENTS

Use of the Advanced Photon Source was supported by the U.S. Department of Energy, Office of Science, Office of Basic Energy Sciences, under contract number W-31-109-Eng-38. We thank Drs. Robert S. Hodges (University of Colorado) and Li-Huei Tsai (Massachusetts Institute of Technology) for helpful discussions and Drs. H. Arai and J. Aoki (University of Tokyo) for the Ndel1 clones. We thank the staff of the European Synchrotron Radiation Facility for help during data collection. This work was supported in part by a National Institutes of Health grant NS 036267 to Z.S.D. and by a grant from the Telethon Foundation to A.M.

Received: July 27, 2007
Revised: September 11, 2007
Accepted: September 13, 2007
Published: November 13, 2007

REFERENCES

Beckwith, S.M., Roghi, C.H., and Morris, N.R. (1995). The genetics of nuclear migration in fungi. Genet. Eng. (N. Y.) *17*, 165–180.

Brandon, N.J., Handford, E.J., Schurov, I., Rain, J.C., Pelling, M., Duran-Jimeniz, B., Camargo, L.M., Oliver, K.R., Beher, D., Shearman, M.S., et al. (2004). Disrupted in Schizophrenia 1 and Nudel form a neurodevelopmentally regulated protein complex: implications for schizophrenia and other major neurological disorders. Mol. Cell. Neurosci. *25*, 42–55.

Bricogne, G., Vonrhein, C., Flensburg, C., Schiltz, M., and Paciorek, W. (2003). Generation, representation and flow of phase information in structure determination: recent developments in and around SHARP 2.0. Acta Crystallogr. D Biol. Crystallogr. *59*, 2023–2030.

Brown, J.H., Cohen, C., and Parry, D.A. (1996). Heptad breaks in α-helical coiled coils: stutters and stammers. Proteins *26*, 134–145.

Brown, J.H., Zhou, Z., Reshetnikova, L., Robinson, H., Yammani, R.D., Tobacman, L.S., and Cohen, C. (2005). Structure of the mid-region of tropomyosin: bending and binding sites for actin. Proc. Natl. Acad. Sci. USA *102*, 18878–18883.

CCP4 (Collaborative Computational Project, Number 4) (1994). The CCP4 suite: programs for protein crystallography. Acta Crystallogr. D Biol. Crystallogr. *50*, 760–763.

Coquelle, F.M., Caspi, M., Cordelieres, F.P., Dompierre, J.P., Dujardin, D.L., Koifman, C., Martin, P., Hoogenraad, C.C., Akhmanova, A., Galjart, N., et al. (2002). LIS1, CLIP-170's key to the dynein/dynactin pathway. Mol. Cell. Biol. *22*, 3089–3102.

Crick, F.H.C. (1953). The packing of alpha-helices: simple coiled-coils. Acta Crystallogr. *6*, 689–697.

Dobyns, W.B., and Truwit, C.L. (1995). Lissencephaly and other malformations of cortical development: 1995 update. Neuropediatrics *26*, 132–147.

Dobyns, W.B., Reiner, O., Carrozzo, R., and Ledbetter, D.H. (1993). Lissencephaly. A human brain malformation associated with deletion of the LIS1 gene located at chromosome 17p13. JAMA *270*, 2838–2842.

Emsley, P., and Cowtan, K. (2004). Coot: model-building tools for molecular graphics. Acta Crystallogr. D Biol. Crystallogr. *60*, 2126–2132.

Fanucci, G.E., and Cafiso, D.S. (2006). Recent advances and applications of site-directed spin labeling. Curr. Opin. Struct. Biol. *16*, 644–653.

Faulkner, N.E., Dujardin, D.L., Tai, C.Y., Vaughan, K.T., O'Connell, C.B., Wang, Y., and Vallee, R.B. (2000). A role for the lissencephaly gene LIS1 in mitosis and cytoplasmic dynein function. Nat. Cell Biol. *2*, 784–791.

Feng, Y., and Walsh, C.A. (2004). Mitotic spindle regulation by Nde1 controls cerebral cortical size. Neuron *44*, 279–293.

Feng, Y., Olson, E.C., Stukenberg, P.T., Flanagan, L.A., Kirschner, M.W., and Walsh, C.A. (2000). LIS1 Regulates CNS lamination by interacting with mNudE, a central component of the centrosome. Neuron *28*, 665–679.

Gonzalez, L., Jr., Brown, R.A., Richardson, D., and Alber, T. (1996a). Crystal structures of a single coiled-coil peptide in two oligomeric states reveal the basis for structural polymorphism. Nat. Struct. Biol. *3*, 1002–1009.

Gonzalez, L., Jr., Plecs, J.J., and Alber, T. (1996b). An engineered allosteric switch in leucine-zipper oligomerization. Nat. Struct. Biol. *3*, 510–515.

Gonzalez, L., Jr., Woolfson, D.N., and Alber, T. (1996c). Buried polar residues and structural specificity in the GCN4 leucine zipper. Nat. Struct. Biol. *3*, 1011–1018.

Hatten, M.E. (2005). LIS-less neurons don't even make it to the starting gate. J. Cell Biol. *170*, 867–871.

Hook, P., and Vallee, R.B. (2006). The dynein family at a glance. J. Cell Sci. *119*, 4369–4371.

Jones, K.L., Gilbert, E.F., Kaveggia, E.G., and Opitz, J.M. (1980). The MIller-Dieker syndrome. Pediatrics *66*, 277–281.

Jones, T.A., Zou, J.Y., Cowan, S.W., and Kjeldgaard, M. (1991). Improved methods for binding protein models in electron density maps and the location of errors in these models. Acta Crystallogr. A Found. Crystallogr. *47*, 110–119.

Langen, R., Oh, K.J., Cascio, D., and Hubbell, W.L. (2000). Crystal structures of spin labeled T4 lysozyme mutants: implications for the interpretation of EPR spectra in terms of structure. Biochemistry *39*, 8396–8405.

Li, J., Lee, W.L., and Cooper, J.A. (2005). NudEL targets dynein to microtubule ends through LIS1. Nat. Cell Biol. *7*, 686–690.

Lupas, A. (1996). Coiled coils: new structures and new functions. Trends Biochem. Sci. *21*, 375–382.

Lupas, A. (1997). Predicting coiled-coil regions in proteins. Curr. Opin. Struct. Biol. *7*, 388–393.

Lupas, A., Van Dyke, M., and Stock, J. (1991). Predicting coiled coils from protein sequences. Science *252*, 1162–1164.

Lupas, A.N., and Gruber, M. (2005). The structure of α-helical coiled coils. Adv. Protein Chem. *70*, 37–78.

Marx, A., Muller, J., and Mandelkow, E. (2005). The structure of microtubule motor proteins. Adv. Protein Chem. *71*, 299–344.

Moitra, J., Szilak, L., Krylov, D., and Vinson, C. (1997). Leucine is the most stabilizing aliphatic amino acid in the d position of a dimeric leucine zipper coiled coil. Biochemistry *36*, 12567–12573.

Mori, D., Yano, Y., Toyo-oka, K., Yoshida, N., Yamada, M., Muramatsu, M., Zhang, D., Saya, H., Toyoshima, Y.Y., Kinoshita, K., et al. (2007). NDEL1 phosphorylation by Aurora-A kinase is essential for centrosomal maturation, separation, and TACC3 recruitment. Mol. Cell. Biol. *27*, 352–367.

Morris, N.R. (2000). Nuclear migration. From fungi to the mammalian brain. J. Cell Biol. *148*, 1097–1101.

Morris, N.R. (2003). Nuclear positioning: the means is at the ends. Curr. Opin. Cell Biol. *15*, 54–59.

Morris, N.R., Xiang, X., and Beckwith, S.M. (1995). Nuclear migration advances in fungi. Trends Cell Biol. *5*, 278–282.

Morris, J.A., Kandpal, G., Ma, L., and Austin, C.P. (2003a). DISC1 (Disrupted-In-Schizophrenia 1) is a centrosome-associated protein that interacts with MAP1A, MIPT3, ATF4/5 and NUDEL: regulation and loss of interaction with mutation. Hum. Mol. Genet. *12*, 1591–1608.

Morris, R.J., Perrakis, A., and Lamzin, V.S. (2003b). ARP/wARP and automatic interpretation of protein electron density maps. Methods Enzymol. *374*, 229–244.

Murshudov, G.N., Vagin, A.A., and Dodson, E.J. (1997). Refinement of macromolecular structures by the maximum-likelihood method. Acta Crystallogr. D Biol. Crystallogr. *53*, 240–255.

Niethammer, M., Smith, D.S., Ayala, R., Peng, J., Ko, J., Lee, M., Morabito, M., and Tsai, L. (2000). NUDEL is a novel Cdk5 substrate that associates with LIS1 and cytoplasmic dynein. Neuron *28*, 697–711.

O'Shea, E.K., Klemm, J.D., Kim, P.S., and Alber, T. (1991). X-ray structure of the GCN4 leucine zipper, a two-stranded, parallel coiled coil. Science *254*, 539–544.

Otwinowski, Z., and Minor, W. (1997). Processing of X-ray diffraction data collected in oscillation mode. Methods Enzymol. *A276*, 307–326.

Rabenstein, M.D., and Shin, Y.K. (1995). Determination of the distance between two spin labels attached to a macromolecule. Proc. Natl. Acad. Sci. USA *92*, 8239–8243.

Reiner, O., Carrozzon, R., Shen, Y., Wehnert, M., Faustinella, F., Dobyns, W.B., Caskey, C.T., and Ledbetter, D.H. (1993). Isolation of a Miller-Dieker lissencephaly gene containing G-protein β-subunits-like repeats. Nature *364*, 717–721.

Sasaki, S., Shionoya, A., Ishida, M., Gambello, M.J., Yingling, J., Wynshaw-Boris, A., and Hirotsune, S. (2000). A LIS1/NUDEL/cytoplasmic dynein heavy chain complex in the developing and adult nervous system. Neuron *28*, 681–696.

Sasaki, S., Mori, D., Toyo-oka, K., Chen, A., Garrett-Beal, L., Muramatsu, M., Miyagawa, S., Hiraiwa, N., Yoshiki, A., Wynshaw-Boris, A., et al. (2005). Complete loss of Ndel1 results in neuronal migration defects and early embryonic lethality. Mol. Cell. Biol. *25*, 7812–7827.

Schneider, T.R., and Sheldrick, G.M. (2002). Substructure solution with SHELXD. Acta Crystallogr. D Biol. Crystallogr. *58*, 1772–1779.

Schroer, T.A. (2004). Dynactin. Annu. Rev. Cell Dev. Biol. *20*, 759–779.

Sheffield, P., Garrard, S., and Derewenda, Z. (1999). Overcoming expression and purification problems of RhoGDI using a family of "Parallel" expression vectors. Protein Expr. Purif. *15*, 34–39.

Shu, T., Ayala, R., Nguyen, M.D., Xie, Z., Gleeson, J.G., and Tsai, L.H. (2004). Ndel1 operates in a common pathway with LIS1 and cytoplasmic dynein to regulate cortical neuronal positioning. Neuron *44*, 263–277.

Smith, D.S., Niethammer, M., Ayala, R., Zhou, Y., Gambello, M.J., Wynshaw-Boris, A., and Tsai, L.H. (2000). Regulation of cytoplasmic dynein behaviour and microtubule organization by mammalian Lis1. Nat. Cell Biol. *2*, 767–775.

Stehman, S.A., Chen, Y., McKenney, R.J., and Vallee, R.B. (2007). NudE and NudEL are required for mitotic progression and are involved in dynein recruitment to kinetochores. J. Cell Biol. *178*, 583–594.

Strelkov, S.V., and Burkhard, P. (2002). Analysis of α-helical coiled coils with the program TWISTER reveals a structural mechanism for stutter compensation. J. Struct. Biol. *137*, 54–64.

Tai, C.Y., Dujardin, D.L., Faulkner, N.E., and Vallee, R.B. (2002). Role of dynein, dynactin, and CLIP-170 interactions in LIS1 kinetochore function. J. Cell Biol. *156*, 959–968.

Tarricone, C., Perrina, F., Monzani, S., Massimiliano, L., Kim, M.H., Derewenda, Z.S., Knapp, S., Tsai, L.H., and Musacchio, A. (2004). Coupling PAF signaling to dynein regulation: structure of LIS1 in complex with PAF-acetylhydrolase. Neuron *44*, 809–821.

Terwilliger, T.C. (2003). Improving macromolecular atomic models at moderate resolution by automated iterative model building, statistical density modification and refinement. Acta Crystallogr. D Biol. Crystallogr. *59*, 1174–1182.

Terwilliger, T.C., and Berendzen, J. (1999). Automated MAD and MIR structure solution. Acta Crystallogr. D Biol. Crystallogr. *55*, 849–861.

Toyo-oka, K., Shionoya, A., Gambello, M.J., Cardoso, C., Leventer, R., Ward, H.L., Ayala, R., Tsai, L.H., Dobyns, W., Ledbetter, D., et al. (2003). 14-3-3epsilon is important for neuronal migration by binding to NUDEL: a molecular explanation for Miller-Dieker syndrome. Nat. Genet. *34*, 274–285.

Toyo-Oka, K., Sasaki, S., Yano, Y., Mori, D., Kobayashi, T., Toyoshima, Y.Y., Tokuoka, S.M., Ishii, S., Shimizu, T., Muramatsu, M., et al. (2005). Recruitment of katanin p60 by phosphorylated NDEL1, an LIS1 interacting protein, is essential for mitotic cell division and neuronal migration. Hum. Mol. Genet. *14*, 3113–3128.

Tripet, B., Wagschal, K., Lavigne, P., Mant, C.T., and Hodges, R.S. (2000). Effects of side-chain characteristics on stability and oligomerization state of a de novo-designed model coiled-coil: 20 amino acid substitutions in position "d". J. Mol. Biol. *300*, 377–402.

Tsai, J.W., Chen, Y., Kriegstein, A.R., and Vallee, R.B. (2005). LIS1 RNA interference blocks neural stem cell division, morphogenesis, and motility at multiple stages. J. Cell Biol. *170*, 935–945.

Vallee, R.B., Williams, J.C., Varma, D., and Barnhart, L.E. (2004). Dynein: an ancient motor protein involved in multiple modes of transport. J. Neurobiol. *58*, 189–200.

Vergnolle, M.A., and Taylor, S.S. (2007). Cenp-f links kinetochores to ndel1/nde1/lis1/dynein microtubule motor complexes. Curr. Biol. *17*, 1173–1179.

Wagschal, K., Tripet, B., Lavigne, P., Mant, C., and Hodges, R.S. (1999). The role of position a in determining the stability and oligomerization state of α-helical coiled coils: 20 amino acid stability coefficients in the hydrophobic core of proteins. Protein Sci. *8*, 2312–2329.

Walshaw, J., and Woolfson, D.N. (2001). Socket: a program for identifying and analysing coiled-coil motifs within protein structures. J. Mol. Biol. *307*, 1427–1450.

Xiang, X., and Fischer, R. (2004). Nuclear migration and positioning in filamentous fungi. Fungal Genet. Biol. *41*, 411–419.

Xu, Q., Ellena, J.F., Kim, M., and Cafiso, D.S. (2006). Substrate-dependent unfolding of the energy coupling motif of a membrane transport protein determined by double electron-electron resonance. Biochemistry *45*, 10847–10854.

Yan, X., Li, F., Liang, Y., Shen, Y., Zhao, X., Huang, Q., and Zhu, X. (2003). Human Nudel and NudE as regulators of cytoplasmic dynein in poleward protein transport along the mitotic spindle. Mol. Cell. Biol. *23*, 1239–1250.

Accession Numbers

The atomic coordinates and structure factors have been deposited with the Protein Data Bank (accession codes 2V71 and 2v66).